fluids

MDPI

Article

Time-Periodic Cooling of Rayleigh–Bénard Convection

Lyes Nasseri [1], Nabil Himrane [2], Djamel Eddine Ameziani [1], Abderrahmane Bourada [3] and Rachid Bennacer [4,*]

1 LTPMP (Laboratoire de Transports Polyphasiques et Milieux Poreux), Faculty of Mechanical and Proceeding Engineering, USTHB (Université des Sciences et de la Technologie Houari Boumedienne), Algiers 16111, Algeria; lyes.nasseri@gmail.com (L.N.); deameziani@usthb.dz (D.E.A.)
2 Labo of Energy and Mechanical Engineering (LEMI), Faculty of Technology, UMBB (Université M'hamed Bougara-Boumerdes, Boumerdes 35000, Algeria; n.himrane@univ-boumerdes.dz
3 Laboratory of Transfer Phenomena, RSNE (Rhéologie et Simulation Numérique des Ecoulements) Team, FGMGP (Faculté de génie Mécaniques et de Génie des Procédés Engineering), USTHB (Université des Sciences et de la Technologie Houari Boumedienne), Bab Ezzouar, Algiers 16111, Algeria; abderrahmanebourada@gmail.com
4 CNRS (Centre National de la Recherche Scientifique), LMT (Laboratoire de Mécanique et Technologie—Labo. Méca. Tech.), Université Paris-Saclay, ENS (Ecole National Supérieure) Paris-Saclay, 91190 Gif-sur-Yvette, France
* Correspondence: rachid.bennacer@ens-paris-saclay.fr

Abstract: The problem of Rayleigh–Bénard's natural convection subjected to a temporally periodic cooling condition is solved numerically by the Lattice Boltzmann method with multiple relaxation time (LBM-MRT). The study finds its interest in the field of thermal comfort where current knowledge has gaps in the fundamental phenomena requiring their exploration. The Boussinesq approximation is considered in the resolution of the physical problem studied for a Rayleigh number taken in the range $10^3 \leq Ra \leq 10^6$ with a Prandtl number equal to 0.71 (air as working fluid). The physical phenomenon is also controlled by the amplitude of periodic cooling where, for small values of the latter, the results obtained follow a periodic evolution around an average corresponding to the formulation at a constant cold temperature. When the heating amplitude increases, the physical phenomenon is disturbed, the stream functions become mainly multicellular and an aperiodic evolution is obtained for the heat transfer illustrated by the average Nusselt number.

Keywords: Rayleigh–Bénard convection; time periodical cooling; Lattice Boltzmann method

Citation: Nasseri, L.; Himrane, N.; Ameziani, D.E.; Bourada, A.; Bennacer, R. Time-Periodic Cooling of Rayleigh–Bénard Convection. *Fluids* **2021**, *6*, 87. https://doi.org/10.3390/fluids6020087

Academic Editor: Marcello Lappa

Received: 19 January 2021
Accepted: 12 February 2021
Published: 16 February 2021

1. Introduction

The building sector is one of the largest energy consuming sectors. It represents a large proportion of total energy consumption, much higher than industry and transport in many countries [1–5]. The major challenge to guarantee good comfort is that energy consumption and the level of comfort are often in conflict in a room [6].

In a confined space, thermal comfort depends on the operation of controlled installations (i.e., heating, ventilation and air conditioning) [7]. Therefore, to assess the energy performance of the building, a thermal analysis is essential in order to predict the thermal responses and calculate building loads (heating/cooling). The key of good thermal comfort is the temperature control. To assess it, two models exist: physical or white-box models based on the energy and mass balance equations, and data-driven or black box models based on artificial neural network and developed after sufficient data are available.

In order to propose an adequate design of the indoor environment where people work and live, several papers have been published on the thermal comfort of buildings [8–10]. Rayleigh–Bénard (RB) convection is a classical problem of natural convection. It appears in several applications of engineering and building, such as thermal comfort by using floor heating or ceiling cooling. The other challenge is the energy storing, so either phase change materials or liquid storing are integrated to enhance the thermal building inertia.

Chandrasekhar [11] and Drazin and Reid [12] implemented a full report on the linearization theory. Moreover, many numerical studies of RB natural convection in rectangular enclosures have been carried out for Newtonian fluids [13–15]. Other researchers were interested in the Rayleigh-Bénard convection in viscoplastic fluids leading to numerical and experimental investigations [14–17]. The Rayleigh number (*Ra*) is the parameter that quantifies the intensity of the thermal driving in convection. For sufficiently large *Ra*, Rayleigh–Bénard convection flow becomes turbulent. Significant progress in our understanding of turbulent convection has been obtained by both experimental and numerical studies [18–20]. The Rayleigh–Bénard convection with all the issues illustrated above becomes more complex in the case of time-dependent boundary conditions [21]. The Rayleigh–Bénard problem, with linear temperature increase, was studied by Kaviany [22] and extended later on by Kaviany and Vogel [23], with the inclusion of solute concentration gradients. The solute gradient represents either the phase diagram solute redistribution near phase change interface or the stabilized long-term energy storing solar pound. According to the results of the Rayleigh–Bénard convection studies, a sufficient condition has been found to control the frequency of heat pulsation in order to initiate convection in a periodically heated and cooled cavity from top wall [24].

Aniss et al. [25] have studied the influence of the gravitational modulation on the stability threshold in the case of a Newtonian fluid confined in Hele-Shaw cell and subjected to vertical periodic motion. A time-dependent perturbation expressed in Fourier series has been applied to the wall temperature according to Bhadauria and Bhatia [26]. They found that it is possible to advance or delay the onset of convection. Umavathi [27] also investigated the effect of external modulation on the thermal convection in a porous medium saturated by a nanofluid. It was found in this last study that the low frequency symmetric thermal modulation is destabilizing while moderate and high frequency symmetric modulation is always stabilizing. Recently, Himraneet et al. [28] have studied numerically the Rayleigh–Bénard convection using the Lattice Boltzmann method. The authors considered periodic heating at the lower wall of the cavity. For high values of Rayleigh number, they obtained an unsteady regime in the form of temporal evolution with several frequencies. Abourida et al. [29] have examined Rayleigh–Bénard convection in a square enclosure with a top wall submitted to constant or sinusoidal cold temperature and sinusoidally heated bottom wall. It was observed that by varying the two imposed temperatures, basic differences were noted in comparison to the case of variable hot temperature and that of constant boundary temperature conditions. Raji et al. [30] have presented Rayleigh–Bénard convection inside square enclosure with a time-periodic cold temperature in the top wall. They proved that the variable cooling can lead to a significant improvement in heat transfer compared to constant cooling, particularly at certain low periods. The influence of thermoelectric effect on the Rayleigh–Bénard instability has been well investigated by researchers [31–33].

The literature review has shown that Rayleigh–Bénard's convection problem is still relevant and often considered with constant boundary conditions whereas reality suggests that heating and cooling conditions are modulated over time (i.e., scrolling of the days). In the present study, the problem of time-periodic cooling applied to Rayleigh–Bénard convection is investigated using Lattice Boltzmann method with multiple relaxation time (LBM-MRT). The study finds its interest in the field of thermal comfort where current knowledge has gaps in the fundamental phenomena (theoretical funds) requiring their exploration.

2. Mathematical Formulation

Lattice Boltzmann method was adopted for the resolution of fluid flow and transports phenomena. This method has non-linearity in its mathematical formulation and therefore approximates the temporal variation wall temperature (totally explicitly unsteady). Fluid flow is described as a movement of particles. In two-dimensional domain, the particles' moving is done by distribution functions with DnQm model, where "n" denote dimensions and "m" discrete velocities [34]. In our study, we used D2Q9 model for dynamic field

and D2Q5 for thermal model. Finally, collisions and advection terms are computed by the Boltzmann equation of the distribution functions [35,36]:

$$f_i(x + e_i\delta_t, t + \delta_t) - f_i(x,t) = \Omega(f_i) + \delta_t F_i \tag{1}$$

where f_i is the distribution function with velocity e_i at lattice node x at time t, δ_t is the discrete time step, $\Omega(f_i)$ is the collision operator and F_i is the implemented external forces term. Then, the collision operator in indicial form is as follows:

$$f_i(x + e_i\delta_t, t + \delta_t) - f_i(x,t) = -1/\tau\left[f_i(x,t) - f_i^{eq}(x,t)\right] + \delta_t F_i \tag{2}$$

where f_i^{eq} is the equilibrium function which is expressed by:

$$f_i^{eq} = w_i\rho\left[1 + 3e_i v + 9(e_i v)^2/2 - 3v^2/2\right] \tag{3}$$

The factors w_i are given as: $\left\{\frac{4}{9}, \frac{1}{9}, 0, 0, \frac{1}{9}, \frac{1}{36}, 0, 0, \frac{1}{36}\right\}$, τ is the relaxation time without dimension. The nine discrete velocities are defined as follows:

$$e_i = \begin{cases} (0,0);\ i = 0 \\ c[\cos((i-1)\pi/2), \sin((i-1)\pi/2)];\ i = 1,2,3,4 \\ \sqrt{2}c[\cos((2i-9)\pi/2), \sin((2i-9)\pi/2)];\ i = 5,6,7,8 \end{cases} \tag{4}$$

The collision term is expressed in the Multiple Relaxation Time model (MRT) D'Humières [37], where better stability is observed with a wide range of Prandtl Number values [38].

$$\Omega = -M^{-1}C[m_i(x,t) - m_i^{eq}(x,t)] \tag{5}$$

The flow field formulation becomes:

$$f_i(x + e_i\delta_t, t + \delta_t) - f_i(x,t) = -M^{-1}C[m_i(x,t) - m_i^{eq}(x,t)] + M^{-1}\delta_t(1 - C/2)D \tag{6}$$

where M is the projection matrix of f_i and f_i^{eq} into the moment space. So, the expression of $m = Mf$ and $m^{eq} = Mf^{eq}$ are given by:

$$\begin{pmatrix} \rho \\ e \\ \phi \\ j_x - (\delta_t/2)\rho F_x \\ q_x \\ j_y - (\delta_t/2)\rho F_y \\ q_y \\ p_{xx} \\ p_{xy} \end{pmatrix} = \begin{bmatrix} 1 & 1 & 1 & 1 & 1 & 1 & 1 & 1 & 1 \\ -4 & -1 & -1 & -1 & -1 & 2 & 2 & 2 & 2 \\ 4 & -2 & -2 & -2 & -2 & 1 & 1 & 1 & 1 \\ 0 & 1 & 0 & -1 & 0 & 1 & -1 & -1 & 1 \\ 0 & -2 & 0 & 2 & 0 & 1 & -1 & -1 & 1 \\ 0 & 0 & 1 & 0 & -1 & 1 & 1 & -1 & -1 \\ 0 & 0 & -2 & 0 & 2 & 1 & 1 & -1 & -1 \\ 0 & 1 & -1 & 1 & -1 & 0 & 0 & 0 & 0 \\ 0 & 0 & 0 & 0 & 0 & 1 & -1 & 1 & -1 \end{bmatrix} \begin{pmatrix} f_0 \\ f_1 \\ f_2 \\ f_3 \\ f_4 \\ f_5 \\ f_6 \\ f_7 \\ f_8 \end{pmatrix}. \tag{7}$$

The fluid density ρ, components moment j_x and j_y are the conserved quantities. The six other moments are non-conserved ones and are relaxed linearly in time namely: energy e, energy squared ϕ, energy flux in the two directions q_x, q_Y and diagonal/off-diagonal component of the strain-rate tensor p_{xx}, p_{xy}. The collision operator is carried out in the moment space and in indicial form:

$$m_i^*(x,t) = m_i(x,t) - C[m_i(x,t) - m_i^{eq}(x,t)] \tag{8}$$

For the thermal model, the two-dimensional D2Q5 model with five velocities is used in this work. This model was chosen and validated by several authors in the literature [30]

due to its simplicity and accuracy. The Boltzmann equation with multi-relaxation time can be written as:

$$g_i(x + e_i\delta_t, t + \delta_t) - g_i(x,t) = -N^{-1}E[n_i(x,t) - n_i{}^{eq}(x,t)] \tag{9}$$

where $g_i(x,t)$ is distribution function of temperature, N is projection matrix of g_i and g_i^{eq} into the moment space, and with the same procedure of temperature (first population) $n = Ng$. The transformation matrix N is given by:

$$\begin{pmatrix} n_0 \\ n_1 \\ n_2 \\ n_3 \\ n_4 \end{pmatrix} = \begin{bmatrix} 1 & 1 & 1 & 1 & 1 \\ 0 & 1 & 0 & -1 & 0 \\ 0 & 0 & 1 & 0 & -1 \\ -4 & 1 & 1 & 1 & 1 \\ 0 & 1 & -1 & 1 & -1 \end{bmatrix} \begin{pmatrix} g_0 \\ g_1 \\ g_2 \\ g_3 \\ g_4 \end{pmatrix} \tag{10}$$

The boundary conditions, according to their macroscopic mathematical formulation are illustrated in Figure 1 for velocities:

$$U(0,Y,t) = U(1,Y,t) = U(X,0,t) = U(X,1,t) = 0 \tag{11}$$

$$V(0,Y,t) = V(1,Y,t) = V(X,0,t) = V(X,1,t) = 0 \tag{12}$$

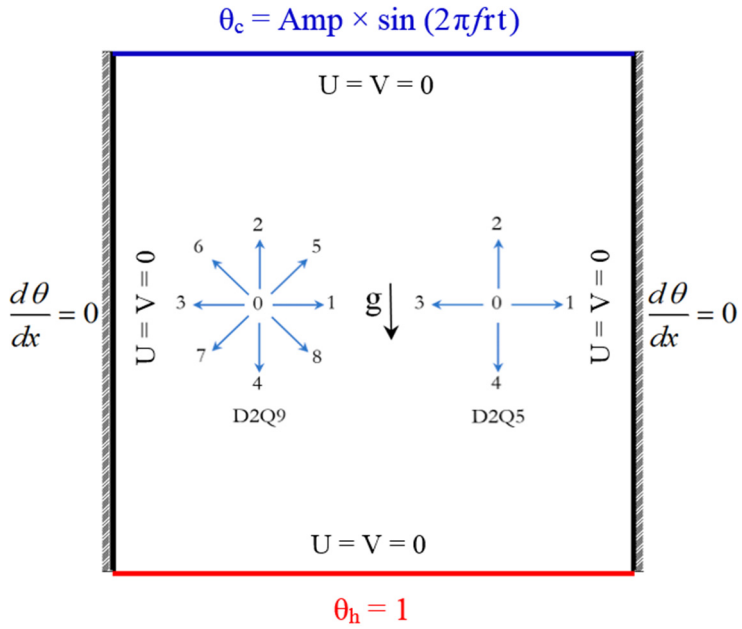

Figure 1. Physical model.

Temperature boundary conditions:

$$\theta(X,1,t) = Amp \cdot \sin(2\pi f t) \tag{13}$$

$$\theta(X,0,t) = 1 \tag{14}$$

$$\left.\frac{\partial\theta(X,Y,t)}{\partial X}\right|_{X=0} = 0 \; and \; \left.\frac{\partial\theta(X,Y,t)}{\partial X}\right|_{X=1} = 0 \tag{15}$$

The instantaneous and average Nusselt number *Nu(t)* at hot and cold wall (*Y = 0* and *Y = 1*) is obtained as:

$$Nu_h(X,0,t) = -\left.\frac{\partial\theta(X,Y,t)}{\partial Y}\right|_{Y=0} and \; Nu_{h_{avg}}(t) = \int_0^1 Nu(X,t)dX \tag{16}$$

$$Nu_c(X,1,t) = -\frac{\partial\theta(X,Y,t)}{\partial Y}\bigg|_{Y=1} \; and \; Nu_{c_{avg}}(t) = \int_0^1 Nu(X,t)dX \tag{17}$$

Before presenting the different results obtained, it is necessary to test the validity of our digital code. Thus, we compared the results of our simulations with those of the various studies carried out on the analysis of Rayleigh–Bénard convection in square cavities filled with air. Different discretization methods have been adopted by these reference studies. Table 1 quantitatively summarizes the values of the average Nusselt number obtained as a function of thermal gradient intensity imposed and characterized by the Rayleigh number. We note that our results show good agreement with those of the literature. The code is also successfully validated for the case of time-periodic temperature condition. Figure 2 shows a good agreement between the present hot and cold Nusselt numbers as function of time and those of Wang et al. [39].

Table 1. Nusselt numbers' validation.

References	Ra			
	10^3	10^4	10^5	10^6
Present Work	1.0035	2.1502	3.912	6.321
Ourtatani et al. [13]	1.0004	2.158	3.910	6.309
Turan [14]	1.0000	2.154	3.907	6.309
Bouabdallah et al. [40]	1.0000	2.2000	3.900	6.400

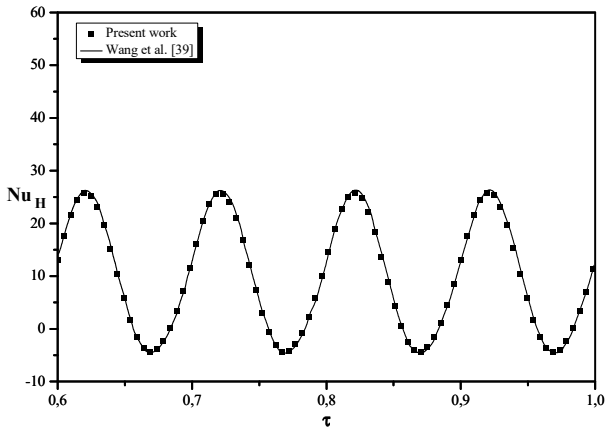

(**a**) Comparison of the average Nusselt number at the hot wall with that of Wang et al. [39].

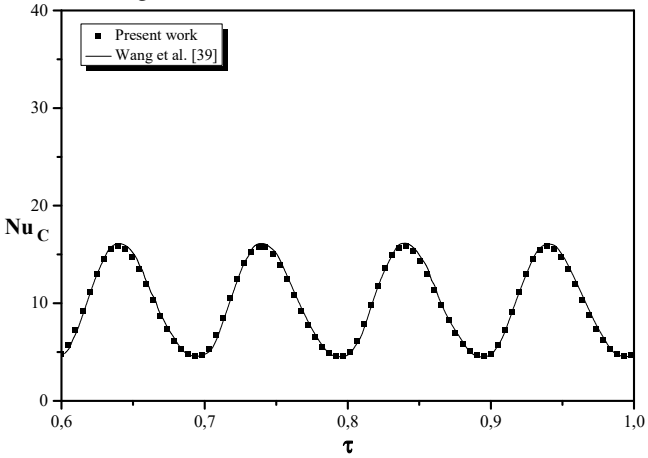

(**b**) Comparison of the average Nusselt number at the cold wall with that of Wang et al. [39].

Figure 2. Time history of Nusselt numbers. Ra = 10^6, Pr = 6.2, τ_p = 0.1 and Amp = 0.8.

In what follows, we present the influence of the various control parameters governing the natural convection problem. The different results are represented in terms of

streamlines, isotherms and heat transfer rate over a time period. Finally, we analyze the periodicity of the convective regime, by means of phase portraits obtained by the heat exchange coefficients.

3. Results

The range of the Rayleigh number values is taken $10^3 \leq \mathrm{Ra} \leq 10^6$. The amplitude of heating is taken between 0.0 and 0.8, and the working fluid is assumed to be air with $\mathrm{Pr} = 0.71$.

In order to better study the behavior of the flow, we varied the amplitude for the three cases, 0.2, 0.5 and 0.8. Figure 3 represents the stream functions for the amplitude 0.2 as a function of the Rayleigh number for the four quarter-period $f = 1/2\pi\tau_p = 1/3 \times 10^{-4}$. Note that the stream function is obtained from the velocity integral and represents the fluid flow rate. When the Rayleigh number is equal to $\mathrm{Ra} = 10^4$, an invariant cell is observed for the four quarter-period.

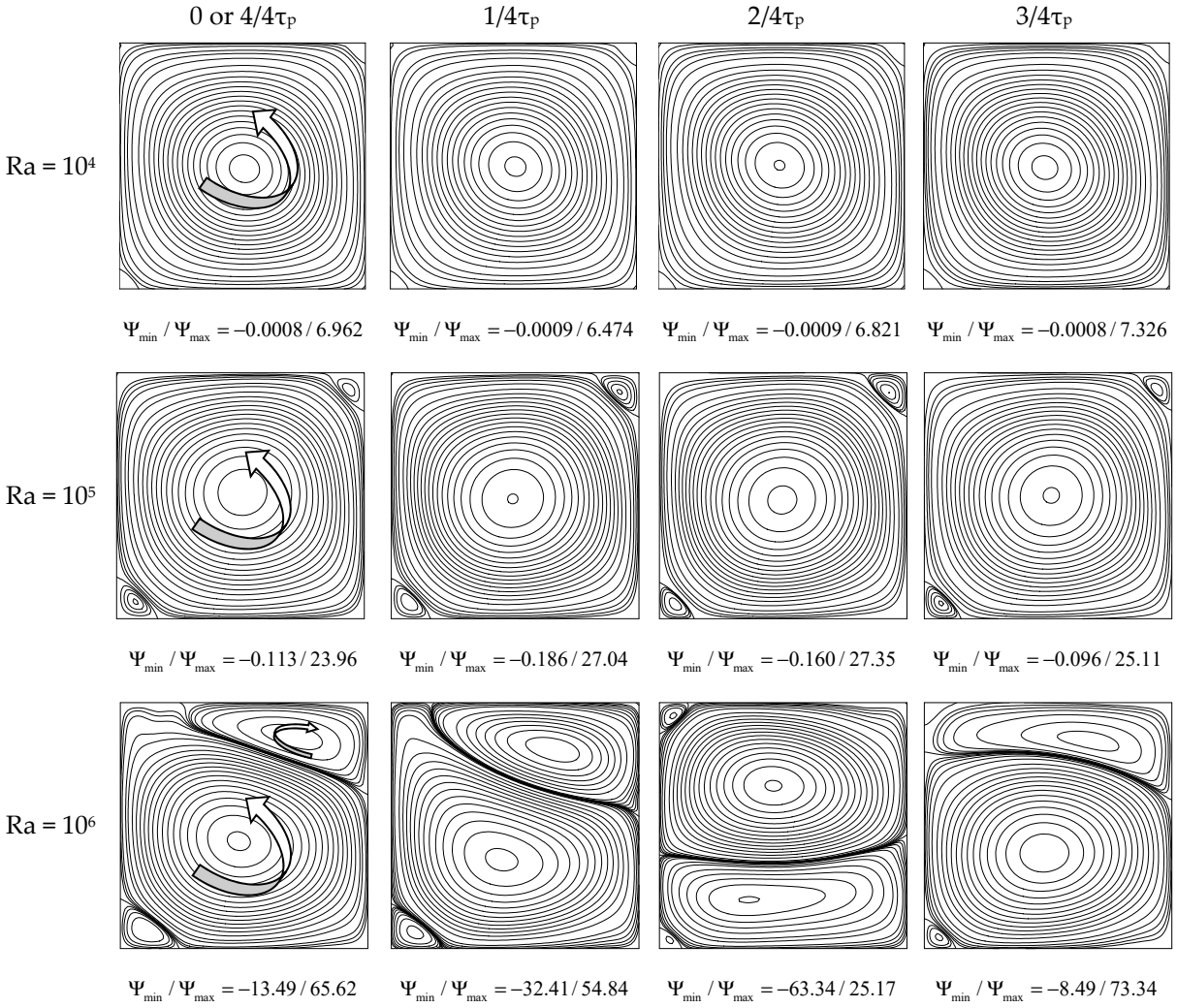

Figure 3. Evolution of streamlines over a period as a function of the Rayleigh number (Amp = 0.2 and $|f| = 0.33 \times 10^{-4}$).

This means that the modulation of cooling has little influence on the dynamic fields. The only difference is that the flow increases characterized by ψ_{max} is increasingly larger than the general temperature gradient is maximum (in the heating period). Same case for the Rayleigh $\mathrm{Ra} = 10^5$ with the presence of small vortices on the upper left and lower right side. As the thermal draft increases, for a Rayleigh number 10^6, the flow loses its

symmetry and subsequently becomes multicellular. For this Rayleigh value and a period of τp/2, the upper secondary cell grew further and took up most of the space of the cavity, in turn becoming counter-rotating bicellular. This spatial multi-cellular (mainly bicellular) competition is persistent throughout the period.

Figures 4 and 5 represent the isocurrents for amplitudes 0.5 and 0.8 respectively, as a function of Rayleigh for the four quarter-period (with $f = 1/3 \times 10^{-4}$). The flow structure for the Rayleigh 10^4 is essentially single-cell, with vortices on the upper right and lower left sides being very small. These findings are similar to the same Rayleigh with a smaller temperature modulation (Amp = 0.2). On the other hand, for Rayleigh equal to 10^5, it is always the same type of flow (i.e., mainly single-cell) but the vortices of the corners are strongly present and influence the size of the main cell. The upper secondary cell still grows ($Ra = 10^6$) and the flow becomes predominantly counter-rotating bicellular and then becomes mainly monocellular again at the end of the period due to the decrease of the upper cell.

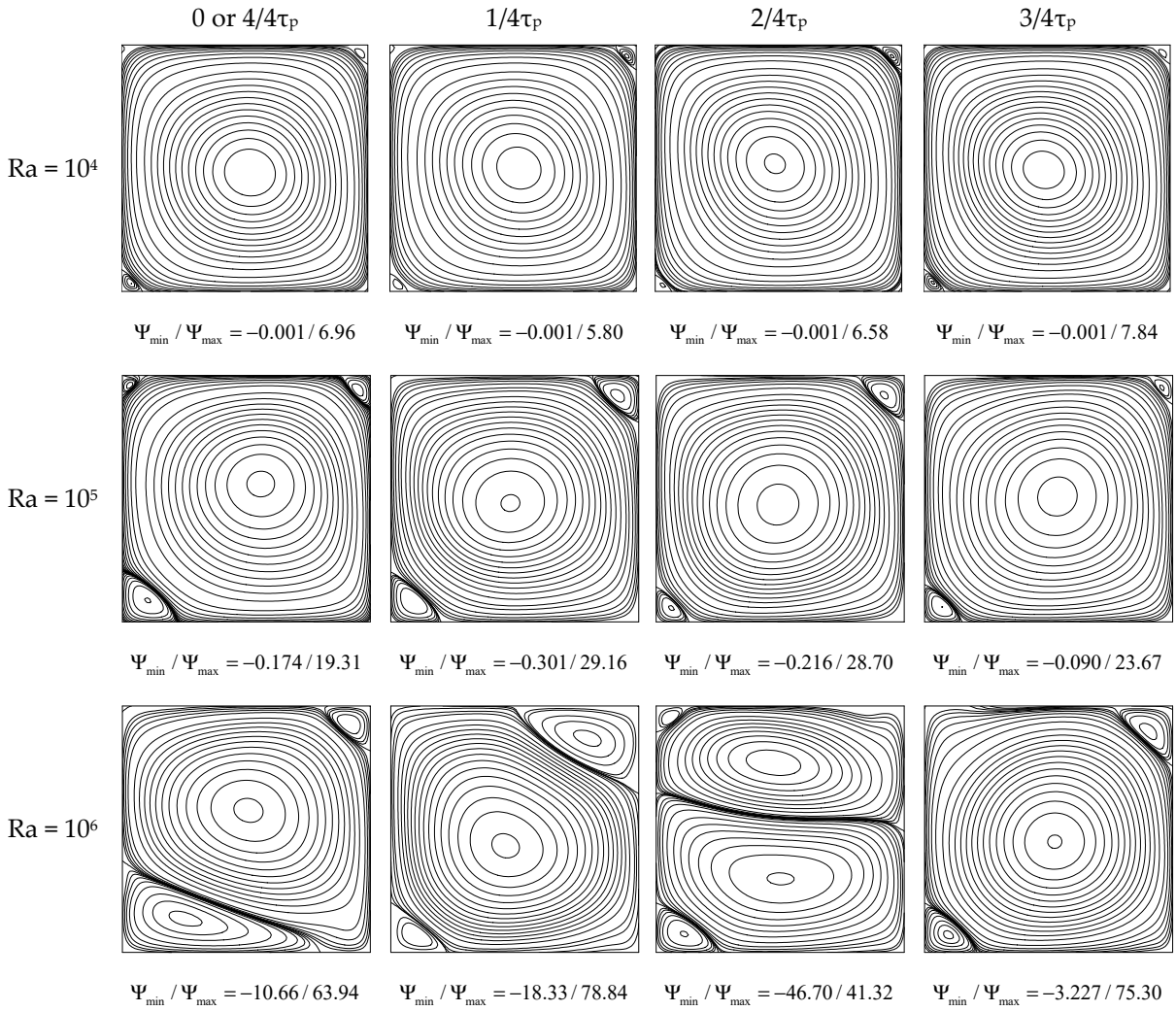

Figure 4. Evolution of streamlines over a period as a function of the Rayleigh number (Amp = 0.5 and $|f| = 0.33 \times 10^{-4}$).

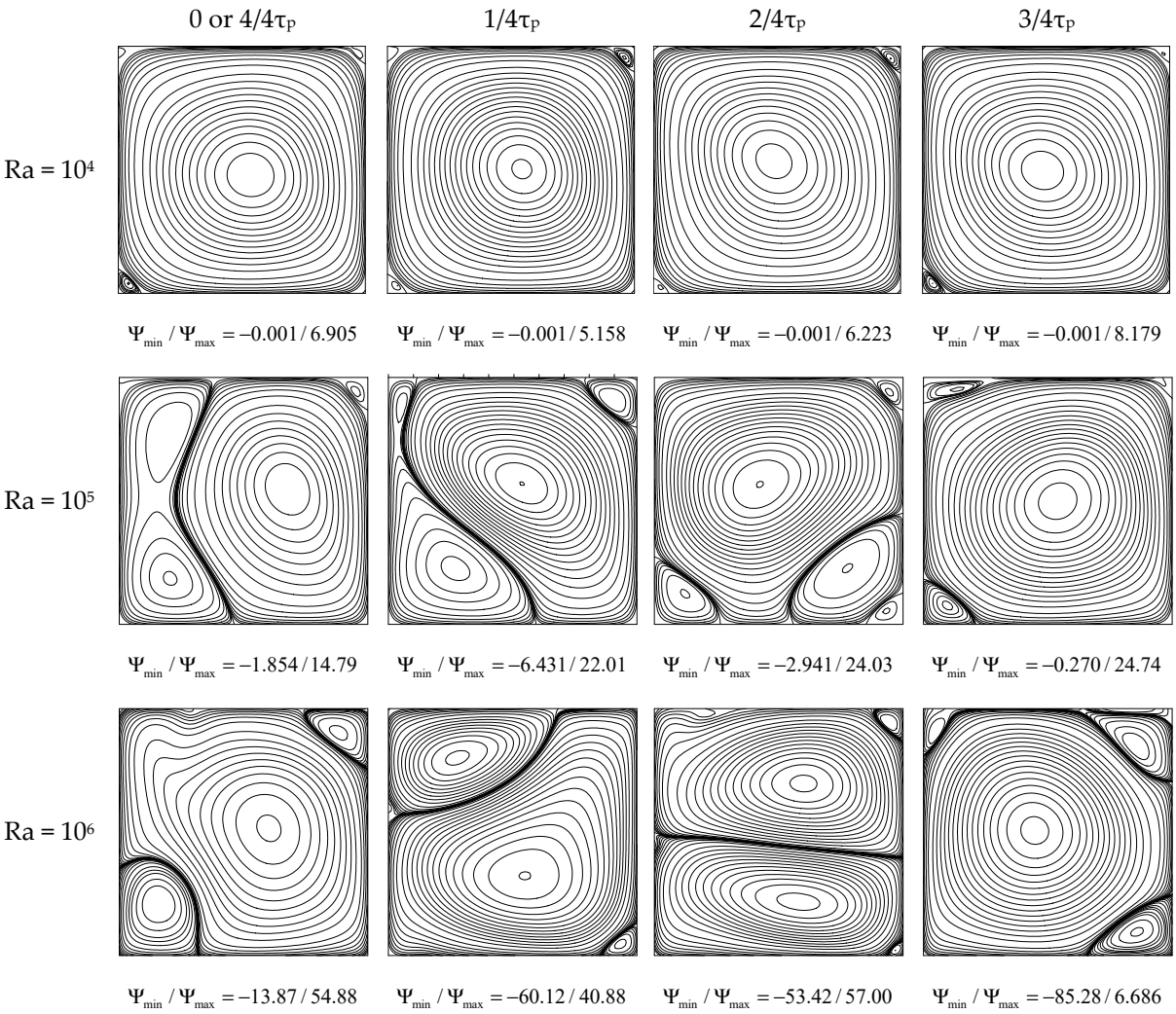

Figure 5. Evolution of streamlines "Ψ" over a period as a function of the Rayleigh number (Amp = 0.8 and $|f| = 0 \times 33\ 10^{-4}$).

Finally, for the temporal step τp, this main cell will be oriented on the right side with one other cell on the lower left side. When the amplitude increases (i.e., Amp = 0.8, Figure 5), an essentially bicellular spatial competition is observed even for Ra = 10^5 and this competition persists even for the maximum Rayleigh of 10^6.

The isotherms corresponding to the different Rayleigh number and the quarter-periods for Amp = 0.2 (Figure 6) show that the heat distribution is consistent with the circulation of the fluid revealed by the stream functions. We also note that the isothermal lines are transported by the movement of fluid. For the Rayleigh 10^3 (not presented in this figure), the isotherms are stratified for all quarter-periods. The isotherms' distortion begins around Ra = 10^4, evolving the form of a vortex. We notice that for Ra = 10^5, isotherms are concentrated on the two horizontal walls for the four beats of the period. When the Rayleigh number reaches to 10^6, we clearly see the conformity of the temperature distribution with respect to the fluid circulation, and distortion is always present for the four-quarter period.

Figure 7 provides evolution of isotherms as function of Rayleigh number and the quarter-period for Amp = 0.8. Visibly, this figure shows that the heat distribution is consistent with the circulation of the fluid revealed by the stream functions. Additionally, we note that the isothermal lines are transported by the fluid flow. For Ra = 10^3(not shown in the figure), isotherms are stratified for all quarter periods, and distortion begins around the Rayleigh value 10^4 in appearance of a vortex. We notice that for Raleigh equal to 10^5,

the temperature lines are found concentrated on the two horizontal walls for the four times of the period.

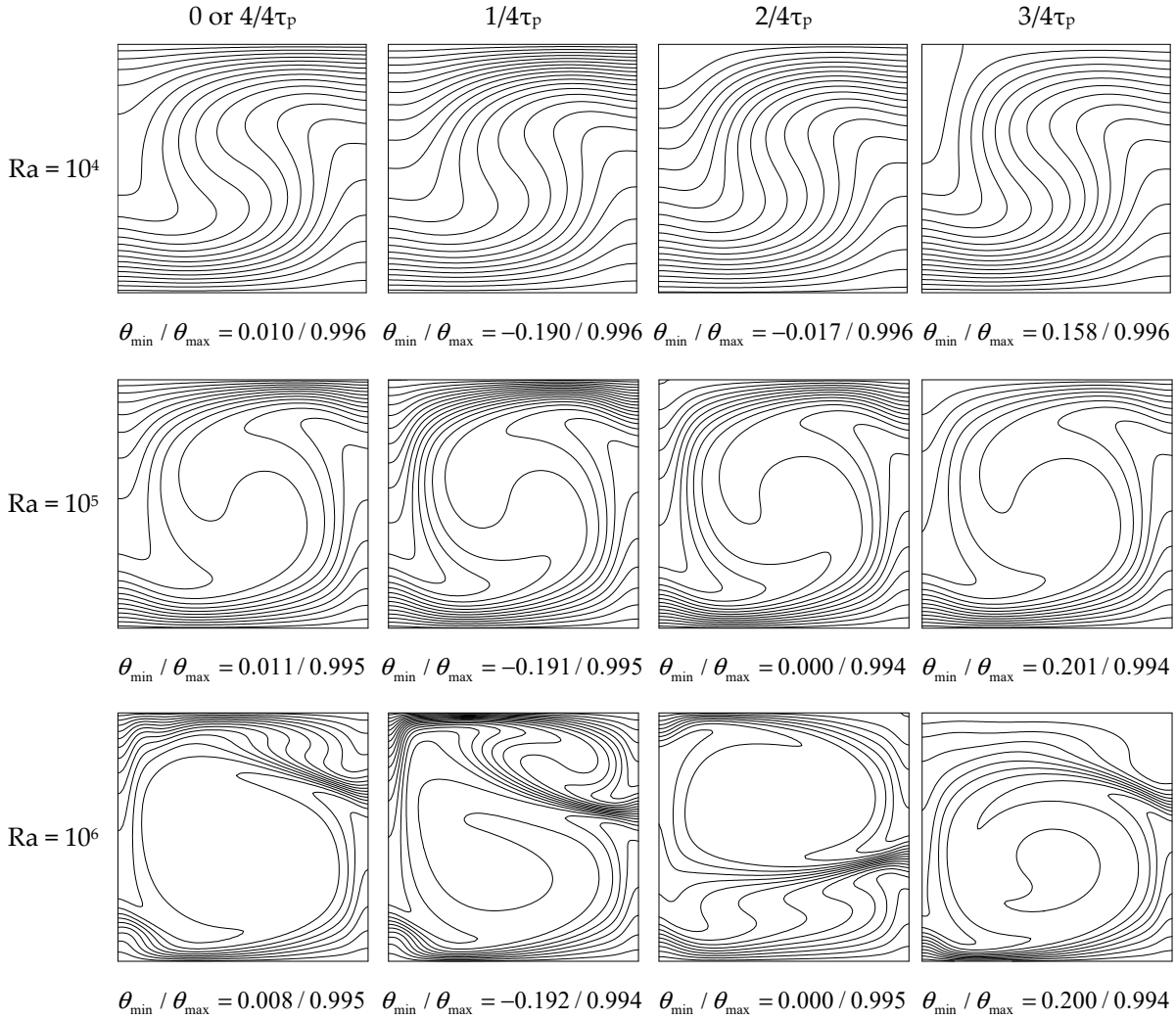

Figure 6. Evolution of isotherms over a period as a function of the Rayleigh number (Amp = 0.2 and $|f| = 0.33 \times 10^{-4}$).

When the Rayleigh reaches to 10^6, we can clearly see the conformity of the temperature distribution with respect to the circulation of the fluid, and the distortion is always present for the four quarters of a period. It can be seen, for the last quarter of a period τp/2, that the temperature lines are concentrated much more on the cold wall compared to that of the opposite side; this is due to a cooling which is more intense.

Figure 8 gives the temporal evolution of the Nusselt number at the cold wall for the last considered periods. The periodic oscillatory regime is established for most Rayleigh numbers. For high Rayleigh numbers, the cold Nusselt curves exhibit quasi-periodic shapes when the cooling modulation amplitude is small (Amp $\leq$ 0.5) and aperiodic shapes for high amplitudes (Amp > 0.5). We note that the more the amplitude increases, the more the heat transfer module intensifies. In the case of Rayleigh 10^6, the curve loses its periodicity due to the appearance of unsteady phenomena. Note that when the amplitude increases, instabilities appear even for the intermediate Rayleigh numbers and lower than Ra < 10^6. Additionally, it is apparent that for low modulation amplitudes, the curves have a quasi-symmetrical shape, whereas when the modulation increases, the physical behavior of the cavity is different between heating and cooling. It should also be noted that it is no longer the increase in the Rayleigh number that governs the growth of transfer rate.

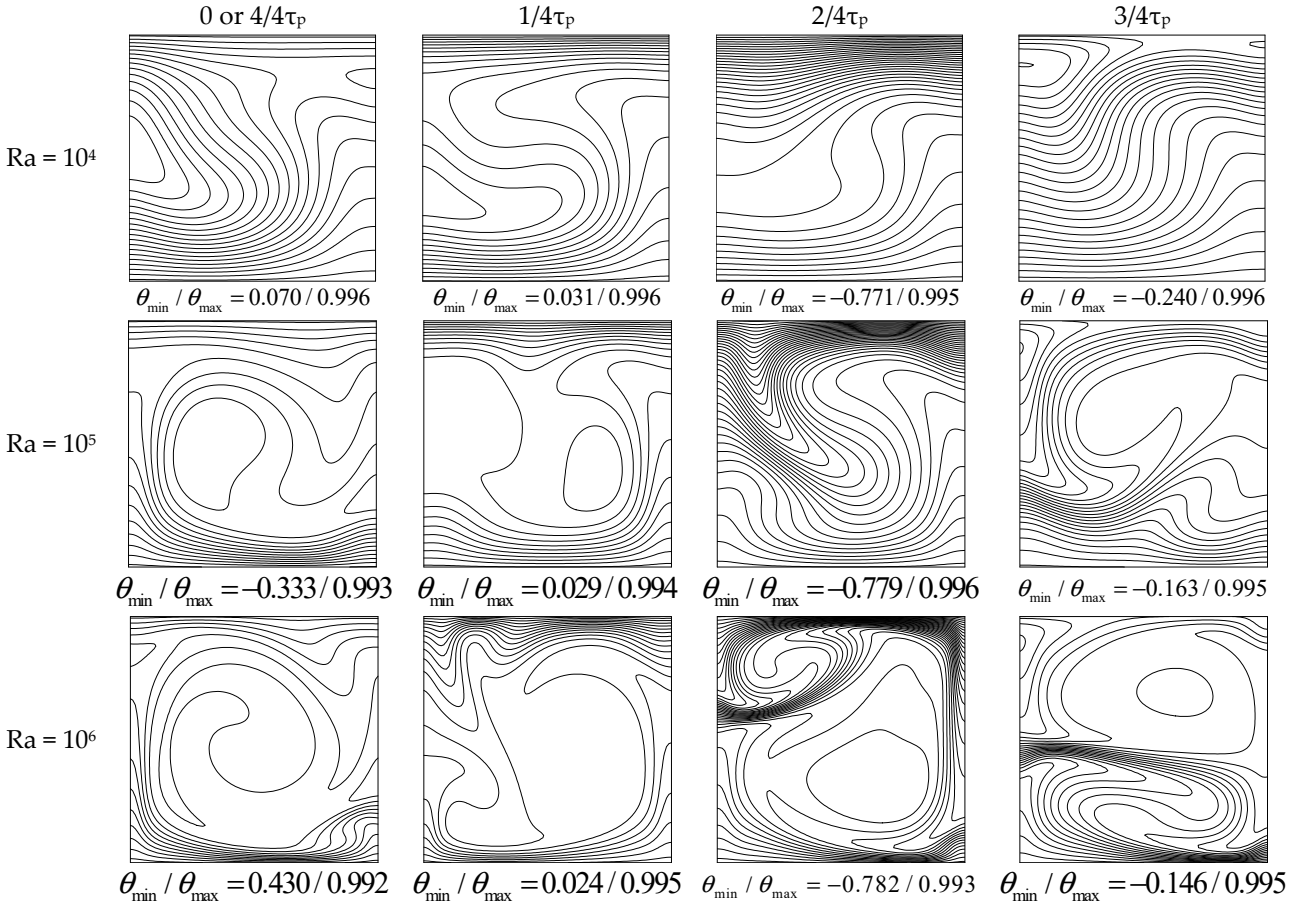

Figure 7. Evolution of isotherms over a period as a function of the Rayleigh number (Amp = 0.8 and $|f| = 0.33 \times 10^{-4}$).

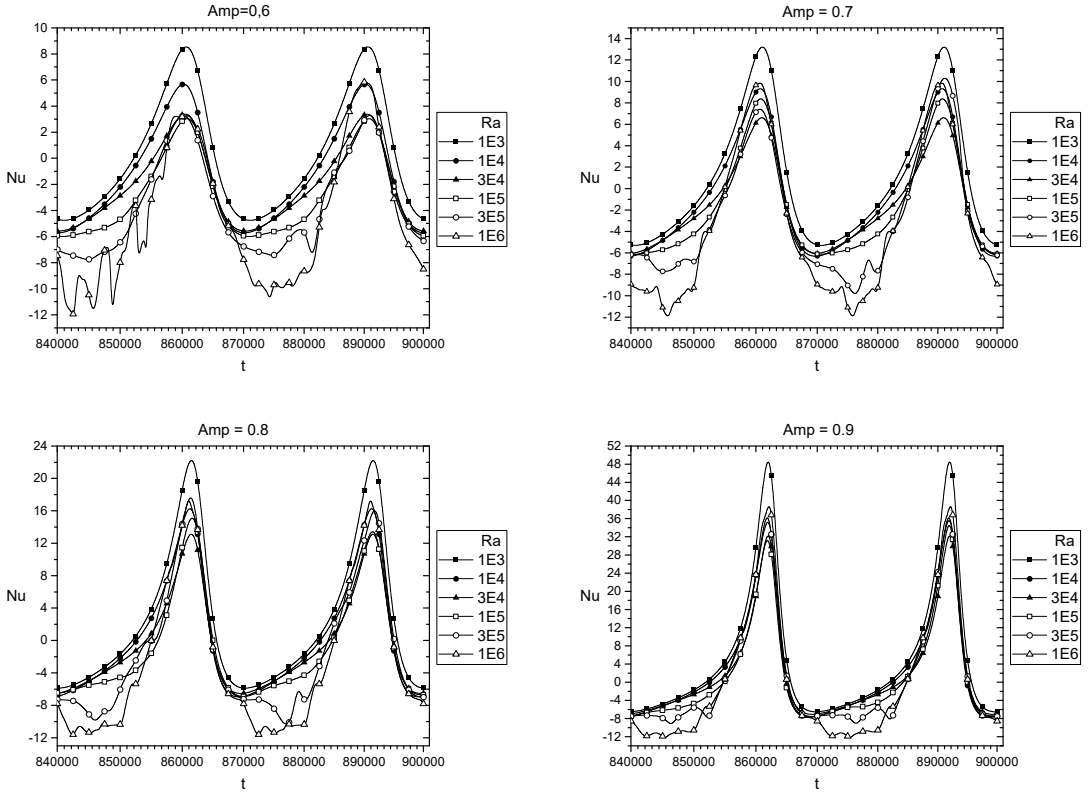

Figure 8. *Cont*.

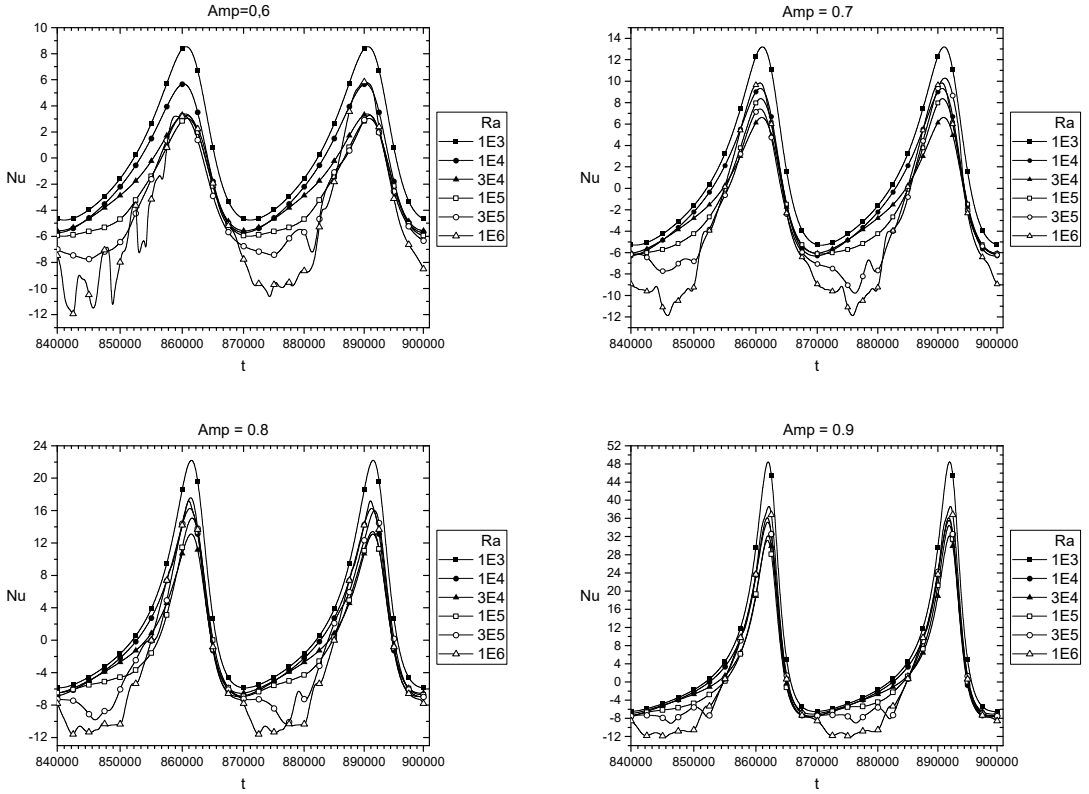

Figure 8. Evolution of the Nusselt number "Nu_c" (at the top wall) as a function of time for different Ra over the last two periods.

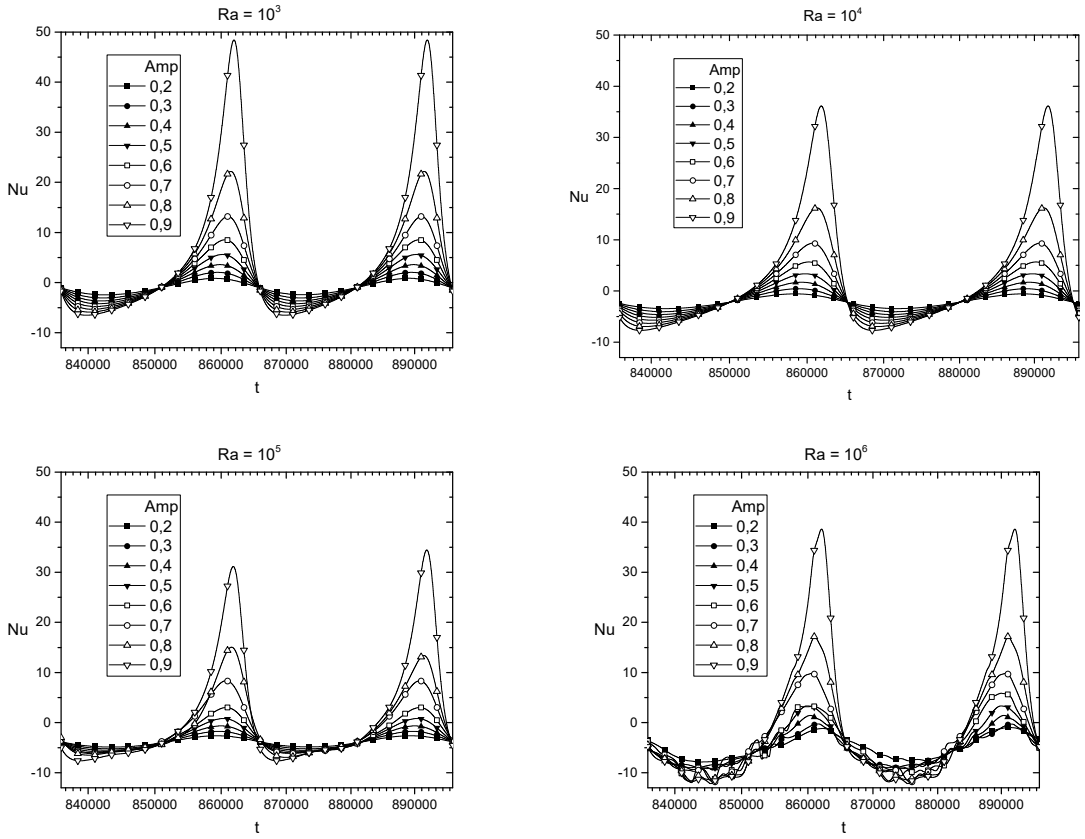

Figure 9. Evolution of the Nusselt number "Nu_c" (at the top wall) as a function of time for different Amp over the last two periods.

Figure 10 illustrates the phase portraits of the normalized Nu_c and Nu_h (cold and hot Nusselt respectively) for different Ra, and for Amp = 0.4 and 0.8, respectively. It is well known that when boundary conditions are not modulated, hot and cold Nusselt numbers must be the same to ensure energy balance. In the case where the boundary conditions are modulated, the heat transfers on the hot and cold sides follow different evolutions [41–44]. The main observation is that for a Rayleigh of 10^3, 10^4 and 10^5, the limit cycle indicates that the regime is periodic; on the other hand for the Rayleigh 10^6, the limit cycle is replaced by a cross cycle indicating the birth of natural instabilities and their addition to the pulsation imposed by the boundary condition. For Amp = 0.8, the limit and cross cycles are stretched diagonally showing that reaching the maximum value of Nu_c induces the fall of Nu_h to its minimum value and vice versa.

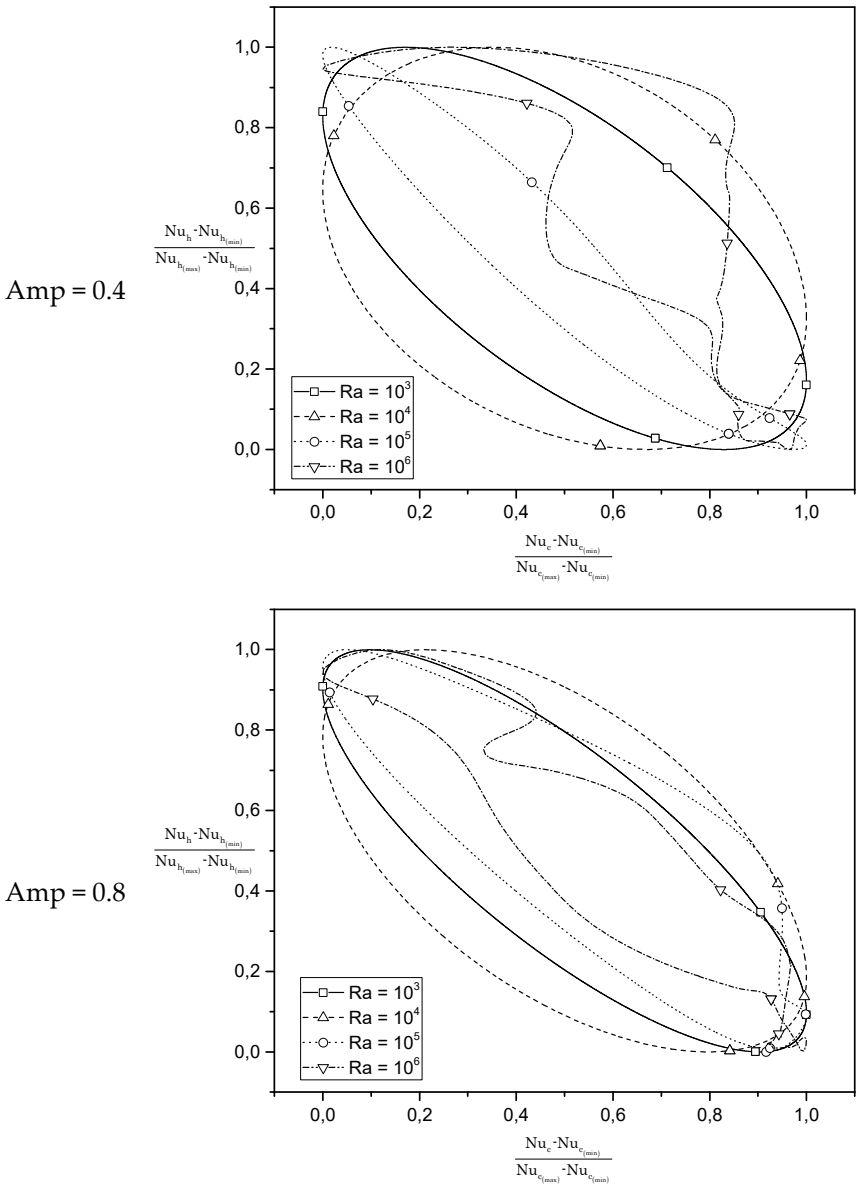

Figure 10. Phase plot for the normalized Nu_c and Nu_h for different Ra (Amp = 0.4 and 0.8).

4. Conclusions

In this study, the Lattice Boltzmann method has been used in order to investigate Rayleigh–Bénard convection in square cavity submitted to a time-periodic cooling. The Rayleigh number value considered is between 10^3 and 10^6, while the amplitude varies 0.2 to 0.8 and Prandtl value kept constant at 0.71. The flow state as well as the thermal fields

depends on the values of control parameters (Ra and Amp). For the dynamic field, the obtained results show that the flow structure changes from predominantly monocellular to predominantly counter-rotating bicellular flow for Rayleigh number values Ra= 10^6 and low values of the heating amplitude. This phenomenon was obtained for lower Rayleigh values (Ra = 10^4) by increasing the value of the heating amplitude.

The analysis of the heat transfer show that for small values of amplitude heating, the averaged Nusselt curves follow a periodic evolution around an average corresponding to the formulation according to a constant cold temperature. An unsteady evolution is observed when the thermal draft increases; this unsteadiness has appeared for low Rayleigh numbers by increasing the value of the heating amplitude.

Author Contributions: Conceptualization, D.E.A.; Formal analysis, L.N., N.H., D.E.A. and R.B.; Investigation, L.N. and N.H.; Methodology, L.N. and N.H.; Supervision, R.B.; Writing—original draft, L.N.; Writing—review & editing, N.H., D.E.A. and A.B. All authors have read and agreed to the published version of the manuscript.

Funding: This research received no external funding.

Institutional Review Board Statement: Not applicable.

Informed Consent Statement: Not applicable.

Data Availability Statement: No data available.

Acknowledgments: The authors acknowledge the financial support of the General Direction of Scientific Research and Technological Development (DGRSDT), Algeria.

Conflicts of Interest: The authors declare that they have no conflict of interest.

Abbreviations

C	Lattice speed
c_s	Sound speed ($c_s = 1/\sqrt{3}$)
c_i	Micro-discrete velocities
f	Frequence
f	Distribution function of momentum equation
f^{eq}	Distribution function for equilibrium momentum equations
G	Gravitational acceleration (m/s^2)
g	Thermal distribution function
H	Convective exchange coefficient
$\overline{H}$	Correction term
J	Components of momentum
L	Cavity length (m)
m	Moments
m^{eq}	Equilibrium moments
M	Transformation matrix
N	Thermal transformation matrix
Nu	Average Nusselt number
Nu_x	Local Nusselt number
Pr	Prandtl number $\Pr = \upsilon/\alpha$
r_j	Position node
Ra	Rayleigh number $Ra = \left(g\,\beta\,\Delta T_{ref} L^3\right)/(\upsilon\,\alpha)$
S	Matrix with S_j diagonal relaxation rates elements
t	Lattice time
t_k	Time at a step k
T	Dimensional temperature
U	Dimensionless horizontal velocity component
V	Dimensionless vertical velocity component
x	Dimensional longitudinal coordinate
y	Dimensional vertical coordinate

X	Dimensionless longitudinal coordinate
Y	Dimensionless vertical coordinate
Subscript	
c	Cold
h	Hot
t	Time derivative
Greek symbols	
α	Thermal diffusivity coefficient (m^2/s)
β	Coefficient of thermal expansion (K^{-1})
$\bar{\varepsilon}$	The second order energy
μ	Dynamic viscosity (kg/m/s)
υ	Kinematic viscosity (m^2/s)
δ_t	Time step
Ψ	Dimensionless stream function
τ	Relaxation time
ρ	Density (Kg/m^3)
θ	Dimensionless temperature
Θ	Diagonal relaxation matrix of σ_i
Ψ	Thermal source term vector
φ	Energy flux

References

1. Fiaschi, D.; Bandinelli, R.; Conti, S. A case study for energy issues of public buildings and utilities in a small municipality: Investigation of possible improvements and integration with renewables. *Appl. Energy* **2012**, *97*, 101–114. [CrossRef]
2. Pérez-Lombard, L.; Ortiz, J.; Pout, C. A review on buildings energy consumption information. *Energy Build.* **2008**, *40*, 394–398. [CrossRef]
3. Yang, L.; Yan, H.; Lam, J.C. Thermal comfort and building energy consumption implications—A review. *Appl. Energy* **2014**, *115*, 164–173. [CrossRef]
4. Ameziani, D.; Bennacer, R.; Bouhadef, K.; Azzi, A. Effect of the days scrolling on the natural convection in an open ended storage silo. *Int. J. Therm. Sci.* **2009**, *48*, 2255–2263. [CrossRef]
5. Himrane, N.; Ameziani, D.E.; Bouhadef, K.; Bennacer, R. Storage Silos Self Ventilation: Interlinked Heat and Mass Transfer Phenomenon. *Numer. Heat Transf. Part A Appl.* **2014**, *66*, 379–401. [CrossRef]
6. Yang, R.; Wang, L. Multi-objective optimization for decision-making of energy and comfort management in building automation and control. *Sustain. Cities Soc.* **2012**, *2*, 1–7. [CrossRef]
7. Enescu, D. A review of thermal comfort models and indicators for indoor environments. *Renew. Sustain. Energy Rev.* **2017**, *79*, 1353–1379. [CrossRef]
8. Manz, H.; Schaelin, A.; Simmler, H. Airflow patterns and thermal behavior of mechanically ventilated glass double façades. *Build. Environ.* **2004**, *39*, 1023–1033. [CrossRef]
9. Dimoudi, A.; Androutsopoulos, A.; Lykoudis, S. Experimental work on a linked, dynamic and ventilated, wall component. *Energy Build.* **2004**, *36*, 443–453. [CrossRef]
10. De Dear, R.J.; Akimoto, T.; Arens, E.A.; Brager, G.; Candido, C.; Cheong, K.W.D.; Li, B.; Nishihara, N.; Sekhar, S.C.; Tanabe, S.; et al. Progress in thermal comfort research over the last twenty years. *Indoor Air* **2013**, *23*, 442–461. [CrossRef]
11. Chandrasekhar, S. *Hydrodynamic and Hydromagnetic Stability*; Oxford University Press: London, UK, 1961.
12. Drazin, P.; Reid, W.; Busse, F.H. Hydrodynamic Stability. *J. Appl. Mech.* **1982**, *49*, 467–468. [CrossRef]
13. Ouertatani, N.; Cheikh, N.B.; Beya, B.B.; Lili, T. Numerical simulation of two-dimensional Rayleigh–Bénard convection in an enclosure. *Comptes Rendus Mécanique* **2008**, *336*, 464–470. [CrossRef]
14. Turan, O.; Chakraborty, N.; Poole, R.J. Laminar Rayleigh-Bénard convection of yield stress fluids in a square enclosure. *J. Non-Newtonian Fluid Mech.* **2012**, *171*, 83–96. [CrossRef]
15. Park, H. Rayleigh–Bénard convection of nanofluids based on the pseudo-single-phase continuum model. *Int. J. Therm. Sci.* **2015**, *90*, 267–278. [CrossRef]
16. Aghighi, M.S.; Ammar, A.; Metivier, C.; Gharagozlu, M. Rayleigh-Bénard convection of Casson fluids. *Int. J. Therm. Sci.* **2018**, *127*, 79–90. [CrossRef]
17. Kebiche, Z.; Castelain, C.; Burghelea, T. Experimental investigation of the Rayleigh–Bénard convection in a yield stress fluid. *J. Non-Newton. Fluid Mech.* **2014**, *203*, 9–23. [CrossRef]
18. Chavanne, X.; Chilla, F.; Chabaud, B.; Castaing, B.; Hebral, B. Turbulent Rayleigh–Bénard convection in gaseous and liquid He. *Phys. Fluids* **2001**, *13*, 1300–1320. [CrossRef]
19. Chillà, F.; Schumacher, J. New perspectives in turbulent Rayleigh-Bénard convection. *Eur. Phys. J. E* **2012**, *35*, 58. [CrossRef]
20. Zhu, X.; Mathai, V.; Stevens, R.J.A.M.; Verzicco, R.; Lohse, D. Transition to the Ultimate Regime in Two-Dimensional Rayleigh-Bénard Convection. *Phys. Rev. Lett.* **2018**, *120*, 144502. [CrossRef]

21. Bhadauria, B.S. Time-periodic heating of Rayleigh–Benard convection in a vertical magnetic field. *Phys. Scr.* **2006**, *73*, 296–302. [CrossRef]
22. Kaviany, M. Onset of Thermal Convection in a Fluid Layer Subjected to Transient Heating From Below. *J. Heat Transf.* **1984**, *106*, 817–823. [CrossRef]
23. Kaviany, M.; Vogel, M. Effect of Solute Concentration Gradients on the Onset of Convection: Uniform and Nonuniform Initial Gradients. *J. Heat Transf.* **1986**, *108*, 776–782. [CrossRef]
24. Lage, J. Convective currents induced by periodic time-dependent vertical density gradient. *Int. J. Heat Fluid Flow* **1994**, *15*, 233–240. [CrossRef]
25. Aniss, S.; Souhar, M.; Belhaq, M. Asymptotic study of the convective parametric instability in Hele-Shaw cell. *Phys. Fluids* **2000**, *12*, 262–268. [CrossRef]
26. Bhadauria, B.S.; Bhatia, P.K. Time-periodic Heating of Rayleigh-Benard Convection. *Phys. Scr.* **2002**, *66*, 59–65. [CrossRef]
27. Umavathi, J.C. Rayleigh–Benard convection subject to time dependent wall temperature in a porous medium layer saturated by a nanofluid. *Meccanica* **2015**, *50*, 981–994. [CrossRef]
28. Himrane, N.; Ameziani, D.E.; Nasseri, L. Study of thermal comfort: Numerical simulation in a closed cavity using the lattice Boltzmann method. *SN Appl. Sci.* **2020**, *2*, 1–7. [CrossRef]
29. Abourida, B.; Hasnaoui, M.; Douamna, S. Transient Natural Convection in a Square Enclosure with Horizontal Walls Submitted to Periodic Temperatures. *Numer. Heat Transf. Part A Appl.* **1999**, *36*, 737–750. [CrossRef]
30. Raji, A.; Hasnaoui, M.; Firdaouss, M.; Ouardi, C. Natural Convection Heat Transfer Enhancement in a Square Cavity Periodically Cooled from Above. *Numer. Heat Transf. Part A Appl.* **2013**, *63*, 511–533. [CrossRef]
31. Eidel'Man, E.D. Excitation of an electric instability by heating. *Physics-Uspekhi* **1995**, *38*, 1231–1246. [CrossRef]
32. Éidel'Man, E.D. Influence of the thickness of the liquid layer on the ratio of the dimensions of a convection cell. *Tech. Phys.* **1998**, *43*, 1275–1279. [CrossRef]
33. Nevskii, S.; Sarychev, V.; Konovalov, S.; Granovskii, A.; Gromov, V. Formation Mechanism of Micro- and Nanocrystalline Surface Layers in Titanium and Aluminum Alloys in Electron Beam Irradiation. *Metals* **2020**, *10*, 1399. [CrossRef]
34. Mohamad, A. *Lattice Boltzmann Method*; Springer: London, UK, 2011; Volume 70.
35. Guo, Y.; Bennacer, R.; Shen, S.; Ameziani, D.; Bouzidi, M. Simulation of mixed convection in slender rectangular cavity with lattice Boltzmann method. *Int. J. Numer. Methods Heat Fluid Flow* **2010**, *20*, 130–148. [CrossRef]
36. Khali, S.; Nebbali, R.; Ameziani, D.E.; Bouhadef, K. Numerical investigation of non-Newtonian fluids in annular ducts with finite aspect ratio using lattice Boltzmann method. *Phys. Rev. E* **2013**, *87*, 053002. [CrossRef] [PubMed]
37. D'Humieres, D. Generalized Lattice-Boltzmann Equations. In Proceedings of the 18th International Symposium, Rarefied Gas Dynamics, Vancouver, BC, Canada, 26–30 July 1994; pp. 450–458.
38. Lallemand, P.; Luo, L.-S. Theory of the lattice Boltzmann method: Dispersion, dissipation, isotropy, Galilean invariance, and stability. *Phys. Rev. E* **2000**, *61*, 6546–6562. [CrossRef]
39. Wang, G.; Meng, X.; Zeng, M.; Ozoe, H.; Wang, Q.W. Natural Convection Heat Transfer of Copper–Water Nanofluid in a Square Cavity With Time-Periodic Boundary Temperature. *Heat Transf. Eng.* **2013**, *35*, 630–640. [CrossRef]
40. Bouabdallah, S.; Ghernaout, B.; Teggar, M.; Benchatti, A.; Benarab, F.-Z. Onset of Natural Convection and Transition Laminar-Oscillatory Convection Flow in Rayleigh-Bénard Configuration. *Int. J. Heat Technol.* **2016**, *34*, 151–157. [CrossRef]
41. Kwak, H.S.; Hyun, J.M. Natural convection in an enclosure having a vertical sidewall with time-varying temperature. *J. Fluid Mech.* **1996**, *329*, 65–88. [CrossRef]
42. Soong, C.; Tzeng, P.; Hsieh, C. Numerical study of bottom-wall temperature modulation effects on thermal instability and oscillatory cellular convection in a rectangular enclosure. *Int. J. Heat Mass Transf.* **2001**, *44*, 3855–3868. [CrossRef]
43. Kazmierczak, M.; Chinoda, Z. Buoyancy-driven flow in an enclosure with time periodic boundary conditions. *Int. J. Heat Mass Transf.* **1992**, *35*, 1507–1518. [CrossRef]
44. Wang, Q.-W.; Wang, G.; Zeng, M.; Ozoe, H. Upward Heat Flux through the Horizontal Fluid Layer of Water with Sinusoidal Wall Temperature at the Top or Bottom Boundary. *Numer. Heat Transf. Part A Appl.* **2007**, *52*, 817–829. [CrossRef]